Acta Crystallographica Section A
Foundations of Crystallography
ISSN 0108-7673

Received 12 October 1999
Accepted 6 January 2000

Triplet-phase measurements using reference-beam X-ray diffraction

Qun Shen,[a,b]* Stefan Kycia[a] and Ivan Dobrianov[c]

[a]Cornell High Energy Synchrotron Source (CHESS), Cornell University, Ithaca, NY 14853, USA, [b]Department of Materials Sciences and Engineering, Cornell University, Ithaca, NY 14853, USA, and [c]Department of Physics, Laboratory of Atomic and Solid State Physics, Cornell University, Ithaca, NY 14853, USA. Correspondence e-mail: qs11@cornell.edu

Reference-beam diffraction (RBD) is a recently developed phase-sensitive X-ray diffraction technique that incorporates the principle of multiple-beam diffraction into the standard oscillating-crystal data-collection method [Shen (1998). *Phys. Rev. Lett.* **80**, 3268–3271]. Using this technique, a large number of multiple-beam interference profiles can be recorded simultaneously on an area detector, from which a large number of triplet phases of Bragg reflections can be determined in a crystallography experiment. In this article, both the theoretical developments and the experimental procedures of the RBD technique are described in detail. Approximate theoretical approaches for RBD are outlined and simple analytical expressions are obtained that provide the basis for an automated data-analysis procedure that can be used to extract triplet phases from a large number of measured reference-beam diffraction profiles. Experimental examples are given for a variety of crystals including GaAs, tetragonal lysozyme and AlPdMn quasicrystal, using both image plates and a charge-coupled device (CCD) as the area detector. Possible uses of the measured phases for crystal structure determination are discussed as well as future prospects of the RBD technique.

1. Introduction

X-ray crystallography is a widely used method in structural biology and materials sciences for solving crystal structures with atomic scale resolution. In a typical crystallography experiment, a large number of diffraction peaks or Bragg reflections are recorded on an area detector while rotating or oscillating a crystal specimen (Fig. 1*a*). The intensity recorded for each Bragg reflection depends only on the magnitude of its structure factor and not on its phase, which is also needed to determine the atomic positions in a crystal. This is the fundamental *phase problem* in diffraction and its general solution remains an active area of research (Hendrickson, 1991; Miller *et al.*, 1993; Giacovazzo *et al.*, 1994; Tegze & Faigel, 1996; Elser, 1999).

Recently, we have developed a phase-sensitive reference-beam diffraction (RBD) technique that has the potential to provide a practical solution to the phase problem in crystallography (Shen, 1998, 1999*a*; Shen *et al.*, 1999, 2000). The technique is based on the principle of multiple-beam or three-beam diffraction (MBD), which has been known to contain structural phase information (Hart & Lang, 1961; Colella, 1974; Post, 1977; Chapman *et al.*, 1981; Chang, 1982; Juretschke, 1982; Schmidt & Colella, 1985; Tischler & Batterman, 1986; Shen, 1986; Shen & Colella, 1987; Shen & Finkelstein, 1990; Chang *et al.*, 1991; Weckert *et al.*, 1993; Colella, 1995*a*; Weckert & Hümmer, 1997; Mathiesen *et al.*, 1998; Chang, 1998). In the past, the intensity profiles of the three-beam diffraction are measured one at a time in an experiment, which is very inefficient and time consuming (Weckert & Hümmer, 1997) and seriously limits the practical implications of the technique. The new RBD method, on the other hand, incorporates the principle of multiple-beam diffraction into the most common crystallographic data-collection technique – the oscillating crystal method – and allows a parallel collection of many three-beam interference profiles. It therefore provides a way to measure both the magnitudes and the triplet phases of a large number of Bragg reflections in a time period that is similar to existing crystallographic techniques such as multiple-wavelength anomalous diffraction (Hendrickson, 1991).

As illustrated in Fig. 1, the RBD technique is a simple conceptual modification (Shen, 1998) to the conventional oscillation camera set-up in direct-beam geometry. Instead of being perpendicular to the incident X-ray beam, the oscillation axis in RBD geometry is tilted by the Bragg angle $\theta_{\mathbf{G}}$ of a strong reference reflection, **G**, which is aligned to coincide with the oscillation axis φ. In this way, reflection **G** can be kept fully excited throughout the crystal oscillation and the intensities of *all* Bragg reflections recorded on an area detector

during such an oscillation can be influenced by the interference arising from the **G**-reflected reference wave and thus are sensitive to the relative phases of the reflections involved. A complete reference-beam interference profile is measured by taking multiple exposures while stepping angle θ through the **G**-reflection rocking curve. In this procedure, the reference reflection **G** serves as a single *detour* reflection that is common to *all* Bragg reflections (main or primary reflections) that are recorded on the area detector. This role reversal of the aligned reflection in RBD provides several simplified theoretical and experimental considerations as compared to the conventional ψ-scanning multiple-beam experiments.

The purpose of this article is to provide a comprehensive and thorough description of the RBD technique, both in theory and in experimental procedure. In §2, we outline the theoretical considerations that are necessary to describe a RBD process and to quantitatively fit the RBD intensity profiles and retrieve the phase information. In particular, we compare two approximate approaches, a second-order Born approximation and an expanded distorted-wave approximation, to the results of an exact n-beam dynamical theory (Colella, 1974). These approximate theories provide the basis for simple analytical expressions that can be used in an automated RBD data-analysis procedure for a large number of Bragg reflections. Also included in §2 are several geometrical factors such as Lorentz and polarization factors that may affect the intensities in a RBD experiment. In §§3 and 4, we present through several examples the details of the RBD data-collection technique and data-reduction and analysis methods. The procedures have been established in such a way that existing crystallographic software packages can be applied whenever it is feasible in order to make the RBD technique as automated as possible. Finally, in §5, we present the strategies for making use of the experimentally measured phases and discuss some of the current problems in the RBD experiment and their potential solutions in the near future.

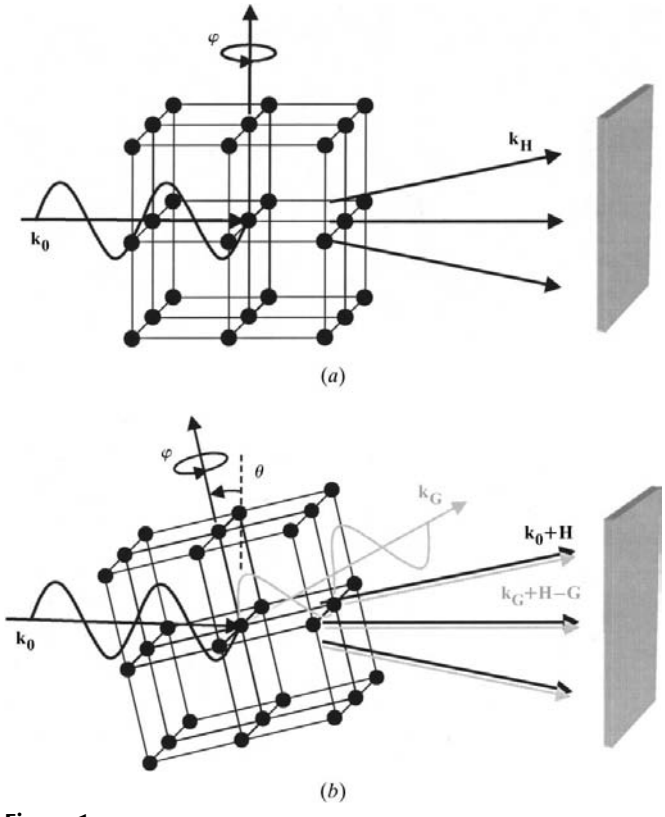

Figure 1
Schematics of (*a*) conventional oscillation set-up used in X-ray crystallography, and (*b*) new reference-beam diffraction in Bragg-inclined geometry, where two sets of diffraction patterns (black and gray) interfere and generate a phase-sensitive diffraction image on an area detector.

2. Theoretical considerations

The three-beam diffraction process that governs a RBD interference involves the reference reflection **G**, a primary reflection **H** and a coupling reflection **H** − **G**. The geometrical condition that the **H** reflection has to satisfy in the reference-beam diffraction process is exactly the same as the one that can be found in the literature for conventional three-beam diffraction (Cole *et al.*, 1962; Caticha-Ellis, 1975). If $\theta_{\mathbf{H}}$ is the Bragg angle for **H** and $\theta_{\mathbf{G}}$ for **G**, then the scattering plane defined by $\mathbf{k_0}$ and **G** must form a specific rotation (oscillation) angle φ with respect to the plane formed by **H** and **G** in order for all three reciprocal nodes, **O**, **G** and **H**, to be on the sphere of reflection simultaneously. It can be shown that this rotation angle φ is given by (Caticha-Ellis, 1975)

$$\cos\varphi = (\sin\theta_H - \cos\beta\sin\theta_G)/\sin\beta\cos\theta_G, \qquad (1)$$

where β is the angle between the **H** and the **G** reciprocal vectors. When $\theta_{\mathbf{G}}$ equals zero, (1) reduces to the condition for the conventional oscillation method in Fig. 1(*a*).

When the geometric RBD condition equation (1) is satisfied, the diffracted intensity $I_{\mathbf{H}}$ for any **H** recorded on the area detector in Fig. 1(*b*) is modified or influenced by the excitation of the **G** reflection and therefore cannot be described by the familiar kinematic theory which is based on the single scattering events only. The goal of this section is to provide a summary of several theories that are suitable for the RBD process along with a few geometric factors that can affect the RBD intensities.

2.1. NBEAM dynamical theory

Since it is intrinsically a three-beam diffraction process, the reference-beam diffraction can be fully described by the NBEAM dynamical theory developed by Colella (1974), with a slight modification. Instead of calculating the diffracted intensity for the 'aligned' reflection **G**, the intensity computation is performed for the reflection **H** that sweeps through the Ewald sphere. In Fig. 2, we show an example of such calculations for GaAs **G** = (004) and **H** = (317), both in thick-crystal Bragg geometry with **G** as the surface normal. The intensities (open circles) in Fig. 2(*a*) are integrated over the oscillation angle φ as in any conventional oscillation image, and are presented as a function of the rocking angle $\Delta\theta = \theta - \theta_{\mathbf{G}}$ of the **G** reflection. An intensity contour map

(on logarithmic scale) is shown in Fig. 2(*b*) as a function of both angles to illustrate the general behavior of three-beam diffraction in reciprocal space.

The intensity profile shown in Fig. 2(*a*) exemplifies the typical three-beam interference pattern that can be measured in a RBD experiment. The interference is sensitive to the phases of the reflections involved, as already illustrated in Colella's original article (Colella, 1974). There are, however, two drawbacks of this rigorous dynamical theory. First, since the theory is based on numerical calculations, it is not easy to visualize the exact phase dependence that exists in the interference effect. Second, considerable computational procedures make it difficult to adapt the theory for any automated data analysis, especially for a large number of Bragg reflections that can be recorded on an area detector in a RBD experiment. We therefore seek alternative approaches that may not be exact as the NBEAM but nonetheless provide analytical expressions with an apparent phase dependence.

Over the years, approximate multiple-beam diffraction theories have been developed by several authors (Juretschke, 1982, 1984; Chang, 1984; Shen, 1986; Thorkildsen, 1987; Thorkildsen & Larsen, 1998; Shen, 1999*b*,*c*). In the following two sections, we outline only two such theories: the second-order Born approximation (Shen, 1986) and the expanded distorted-wave approximation (Shen, 1999*b*,*c*), which has been developed most recently and is tailored specifically for the RBD geometry.

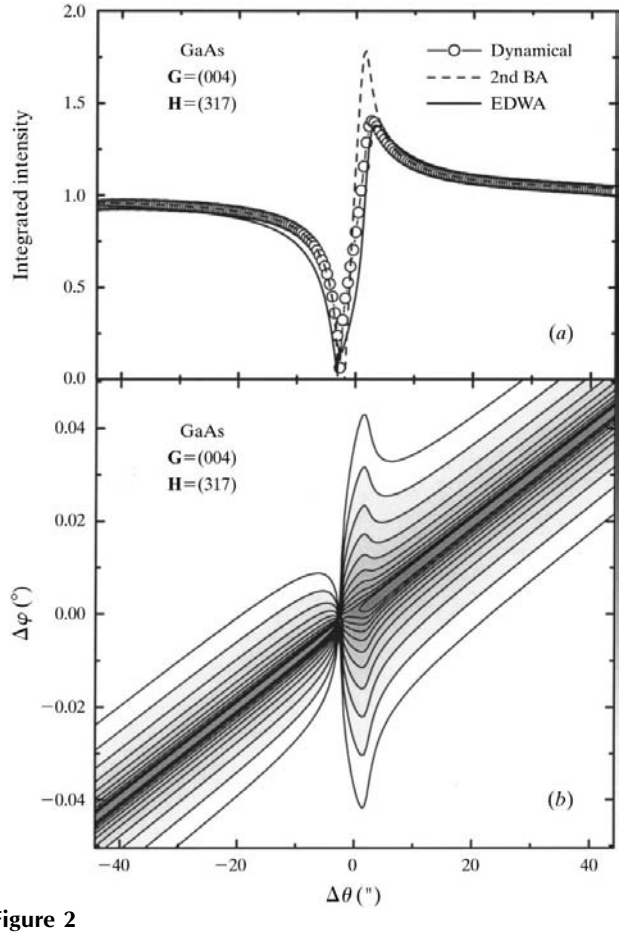

Figure 2
(*a*) Theoretical calculations of a reference-beam diffraction profile using NBEAM dynamical theory (circles), second-order Born approximation (dashed curve) and expanded distorted-wave approximation (EDWA, solid curve). (*b*) Intensity contour map using NBEAM. Both plots are for GaAs, **G** = (004) and **H** = (317).

2.2. Second-order Born approximation

According the standard scattering theories in quantum mechanics and electrodynamics, a scattered X-ray wave field $\mathbf{D}(\mathbf{r})$ from a crystal can be represented by a Born approximation series, with its zeroth-order solution $\mathbf{D}^{(0)}$ being the incident-wave, first-order solution $\mathbf{D}^{(1)}$ being a singly scattered wave in the usual kinematic or two-beam approximation, and second-order solution $\mathbf{D}^{(2)}$ representing a doubly scattered wave with three-beam interactions, and so on (Shen, 1986):

$$\mathbf{D}(\mathbf{r}) = \mathbf{D}^{(0)} + \mathbf{D}^{(1)} + \mathbf{D}^{(2)} + \ldots . \qquad (2)$$

It follows that the conventional oscillating crystal geometry in Fig. 1(*a*) is based on observing the two-beam reflections $\mathbf{D}^{(1)}$ with the rotation axis lined up on the incident beam $\mathbf{D}^{(0)}$, while the reference-beam geometry in Fig. 1(*b*) is automatically set up to observe the three-beam interactions $\mathbf{D}^{(2)}$ with the rotation axis chosen to diffract a reference beam $\mathbf{D}^{(1)}$.

Using the Born-series equation (2), it can be shown (Shen, 1998) that a RBD process can be described within the second-order Born approximation and that the RBD interference effect is sensitive to the *invariant triplet phase*:

$$\delta = \alpha_{\mathbf{H}-\mathbf{G}} + \alpha_{\mathbf{G}} - \alpha_{\mathbf{H}},$$

where the $\alpha_{\mathbf{H}}$'s are the phases of the corresponding structure factors. In addition to δ, the phase of the **G**-reflected wave can be tuned by rocking the tilt angle θ through the **G**-reflection rocking curve, much like in an X-ray standing-wave experiment (Batterman, 1964). Observations of intensity $I_{\mathbf{H}}$ as a function of θ for each of the Bragg reflections recorded on the area detector yields a complete interference profile $I_{\mathbf{H}}(\theta)$, which is given by a normalized intensity (Shen, 1998, 1999*a*):

$$I_{\mathbf{H}}(\theta) = 1 + 2|F_{\mathbf{H}-\mathbf{G}}/F_{\mathbf{H}}|[R_{\mathbf{G}}(\theta)]^{1/2}\cos[\delta + \nu_{\mathbf{G}}(\theta)], \qquad (3)$$

where $R_{\mathbf{G}}(\theta)$ is the reflectivity, $\nu_{\mathbf{G}}(\theta)$ is the dynamical phase shift of the reference reflection **G** and $I_{\mathbf{H}}(\theta)$ has been normalized to the two-beam intensity. We note here that the factor of 2 in equation (3) was missing in Shen's (1998, 1999*a*) papers because of an error in the earlier derivations that $[R_{\mathbf{G}}(\theta)]^{1/2}\exp(i\nu_{\mathbf{G}})/w$, with w being the Darwin width, should be equivalent to $1/(2\Delta\theta)$ instead of $1/\Delta\theta$.

An example of the RBD profiles calculated using equation (3) is shown in Fig. 2(*a*) as a dashed curve. We see that the second-order Born approximation agrees with the NBEAM result very well, except near the center where dynamical effects such as extinction and higher-order multiple scattering dominate. Once the reference reflection **G** is chosen in an experiment, both $R_{\mathbf{G}}(\theta)$ and $\nu_{\mathbf{G}}(\theta)$ in equation (3) are known and common to all reflections recorded on the area detector, and therefore any difference in $I_{\mathbf{H}}(\theta)$ between two recorded reflections is due mostly to the difference in their triplet phases δ.

In practice, the dynamical phase shift $\nu_{\mathbf{G}}(\theta)$ can be approximated by a hyperbolic tangent function (Shen, 1999*a*),

$$\nu_{\mathbf{G}}(\theta) = \pi/2\{1 - \tanh[(\theta - \theta_{\mathbf{G}})/\Delta]\}, \quad (4)$$

which closely resembles the true phase function in dynamical diffraction theory, convoluted with an experimental resolution and/or mosaic spread function of a half-width Δ and centered at $\theta_{\mathbf{G}}$. The reflectivity curve $R_{\mathbf{G}}(\theta)$ can be approximated with a Lorentzian that has the same center and half width Δ as in $\nu_{\mathbf{G}}(\theta)$, as will be discussed in detail in §4.

2.3. Expanded distorted-wave Born approximation

The result based on the second-order Born approximation, equation (3), includes only the interference term in the diffracted intensity and a phase-insensitive magnitude-squared term has been omitted since it is a higher-order term. For a more rigorous description of the reference-beam diffraction, an expanded distorted-wave approximation (EDWA) has been developed (Shen, 1999*b*,*c*). This new approach not only provides the best physical interpretation (Fig. 3) of the RBD process but also yields a quantitative analytical description of the RBD intensities that are almost identical to the full NBEAM dynamical theory (Colella, 1974).

The EDWA approach follows closely the algorithm of the conventional distorted-wave Born approximation for X-ray surface scattering studies (Vineyard, 1982; Dietrich & Wagner, 1984; Sinha *et al.*, 1988), with an important revision that a *sinusoidal* Fourier component **G** is added to the distorting component of the dielectric function (Fig. 3). This sinusoidal component represents the perturbing **G** reflection charge density and the resulting distorted wave is in fact composed of two waves, **O** and **G** waves. Instead of the Fresnel theory used for surface studies, a two-beam dynamical theory (*e.g.* Batterman & Cole, 1964) is employed to evaluate these distorted waves while the subsequent scattering of these waves is again handled by the Born approximation.

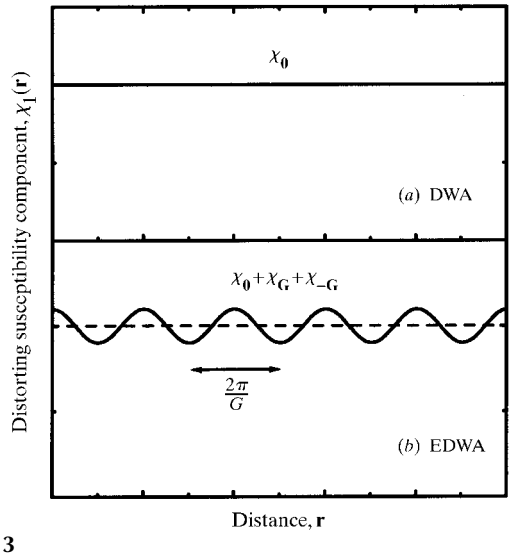

Figure 3
Schematic illustration of the distorting susceptibility in (*a*) conventional distorted-wave approximation (DWA) for surface scattering, and (*b*) expanded distorted-wave approximation (EDWA) for reference-beam diffraction.

Because of the use of dynamical theory in obtaining the distorted waves, the EDWA algorithm allows a rigorous distinction between the Bragg-reflection and the Laue-transmission cases for the reference **G** reflection, whereas, in the Born-approximation calculations of the primary **H** waves, such distinctions are neglected. In both the Bragg and the Laue cases, it can be shown that the diffracted wave field for **H** is given by the following compact expression (Shen, 1999*c*):

$$\mathbf{D}_{\mathbf{H}} = \mathbf{D}_{\mathbf{H}}^{(1)}[r_{\mathbf{0}} + |F_{\mathbf{H-G}}/F_{\mathbf{H}}|r_{\mathbf{G}} \exp(i\delta)],$$

where $\mathbf{D}_{\mathbf{H}}^{(1)}$ is the conventional first-order Born wave field and $r_{\mathbf{0}}$, $r_{\mathbf{G}}$ are the amplitudes of the distorted waves that depend on the diffraction geometry. For example, in a semi-infinite symmetric Bragg case, $r_{\mathbf{0}} = 1$ and $r_{\mathbf{G}} = -[\eta_{\mathbf{G}} \pm (\eta_{\mathbf{G}}^2 - 1)^{1/2}]$, and, in a thin transparent symmetric Laue case, which applies to most situations involving macromolecular crystals, $r_{\mathbf{0}} = \cos(A\eta_{\mathbf{G}}) + i\sin(A\eta_{\mathbf{G}})$ and $r_{\mathbf{G}} = i\sin(A\eta_{\mathbf{G}})/\eta_{\mathbf{G}}$. Here we have used the standard notations, normalized angular parameter $\eta_{\mathbf{G}}$ and *Pendellösung* length A, as in conventional two-beam dynamical theory. Finally, the diffracted intensity $I_{\mathbf{H}}$ for **H** is averaged over thickness t of the crystal: $I_{\mathbf{H}} = (1/t)\int_0^t |\mathbf{D}_{\mathbf{H}}|^2 \, dz$, which takes into account the effect of primary extinction due to **G** in Bragg cases and the *Pendellösung* effect in Laue cases (Shen, 1999*b*,*c*).

In the case of symmetric **G** reflection from a thick crystal, the final intensity is given by the following simple analytical expression (Shen, 1999*b*):

$$I_{\mathbf{H}} = [1 + 2|F_{\mathbf{H-G}}r_{\mathbf{G}}/F_{\mathbf{H}}|\cos(\delta + \nu_{\mathbf{G}}) + |F_{\mathbf{H-G}}r_{\mathbf{G}}/F_{\mathbf{H}}|^2](\mu_0/\mu_z), \quad (5)$$

where μ_0/μ_z is the normalized extinction correction (Authier, 1986) owing to reflection **G**, which is a function of θ and typically resembles an upside-down reflectivity curve.

It should be pointed out that equation (5) includes both the phase-sensitive and the phase-insensitive terms and is valid for all measured Bragg reflections and for the entire excitation range of the reference reflection **G**. The most significant improvements of equation (5) over the second-order Born approximation equation (3) are reflected in the phase-insensitive terms, the squared term and the extinction factor μ_0/μ_z, that contribute most near the center of the **G** rocking curve. An example of the EDWA calculation is shown in Fig. 2(*a*) as the solid curve for GaAs (317)/(004). It has also been shown (Shen, 1999*b*) that the intensities given by equation (5) agree very well with the NBEAM theory for both weak and strong primary reflections. This theory, and its extension to the transmission cases (Shen, 1999*c*), may therefore be used in RBD data analyses to improve the curve-fitting results that yield the triplet-phase values.

2.4. Lorentz factor and angular correction

In a RBD experiment, the intensity of any Bragg reflection **H** is integrated by sweeping the Ewald sphere through the corresponding reciprocal node **H** at a velocity determined by

the effective Lorentz factor, which can be obtained by differentiating equation (1) with respect to $\theta_{\mathbf{H}}$:

$$\Delta\varphi_{\mathbf{H}} = -[\cos\theta_{\mathbf{H}}/(\sin\beta\sin\varphi\cos\theta_{\mathbf{G}})]\Delta\theta_{\mathbf{H}}, \quad (6)$$

where $\Delta\theta_{\mathbf{H}}$ is an angular width owing to mosaicity and crystal domain size. This expression is essentially the same as that given by *e.g.* Zachariasen (1945), except that the Bragg law for **H** has been used to convert the dimension in reciprocal space to the corresponding change in $\theta_{\mathbf{H}}$. Equation (6) provides a way to determine whether a Bragg reflection **H** recorded in a RBD measurement is not completely recorded within a given oscillation range, the so-called 'partials', owing to a very wide $\Delta\varphi_{\mathbf{H}}$ for example.

In addition to the Lorentz factor equation (6), a differentiation of equation (1) with respect to $\theta_{\mathbf{G}}$ provides a reference-beam correction angle $\Delta\varphi_{\mathbf{G}}$. This is the correction to the rotation angle φ, as defined in equation (1), at which **H** is excited when the reference reflection **G** is detuned from its Bragg condition by a deviation angle $\Delta\theta_{\mathbf{G}}$:

$$\Delta\varphi_{\mathbf{G}} = [(\cos\beta - \sin\theta_{\mathbf{H}}\sin\theta_{\mathbf{G}})/(\sin\beta\sin\varphi\cos^2\theta_{\mathbf{G}})]\Delta\theta_{\mathbf{G}}. \quad (7)$$

Equation (7) can be used to explain the tilted trajectory in Fig. 2(*b*) and is useful in estimating the peak-position shifts when multiple frames of oscillation data are collected at slightly different $\theta_{\mathbf{G}}$ positions using, for example, a charge-coupled-device (CCD) X-ray camera. Special care has to be taken for those reflections close to being coplanar ($\varphi \approx 0$) and close to the **G** reciprocal vector ($\beta \approx 0$).

2.5. Polarization effect

Finally, it is obvious that in general the incident polarization for **H** can be different from that for the reference **G** reflection, unless **H** is coplanar to **G**. Assuming that the incident beam consists of a perpendicular polarization for **G**, $\mathbf{D_0} = D_0\boldsymbol{\sigma}$, it can be shown that both $\boldsymbol{\sigma}_{\mathbf{H}}$ and $\boldsymbol{\pi}_{\mathbf{H}}$ components exist in the incident beam for **H** reflection:

$$\mathbf{D_0} = D_0[(\boldsymbol{\sigma}_{\mathbf{H}} + p_{\mathbf{H}}\boldsymbol{\pi}_{\mathbf{H}})/(1 + p_{\mathbf{H}}^2)^{1/2}],$$

where

$$p_{\mathbf{H}} = \sin\varphi/(\cot\beta\cos\theta_{\mathbf{G}} - \cos\varphi\sin\theta_{\mathbf{G}}). \quad (8)$$

Equation (8) shows that the only situation for which $p_{\mathbf{H}} = 0$ is the coplanar case $\varphi = 0$.

It should be noted that the polarization mixing phenomenon that is present in conventional multiple-beam diffraction (Juretschke, 1984; Shen & Finkelstein, 1990, 1992; Shen, 1993)

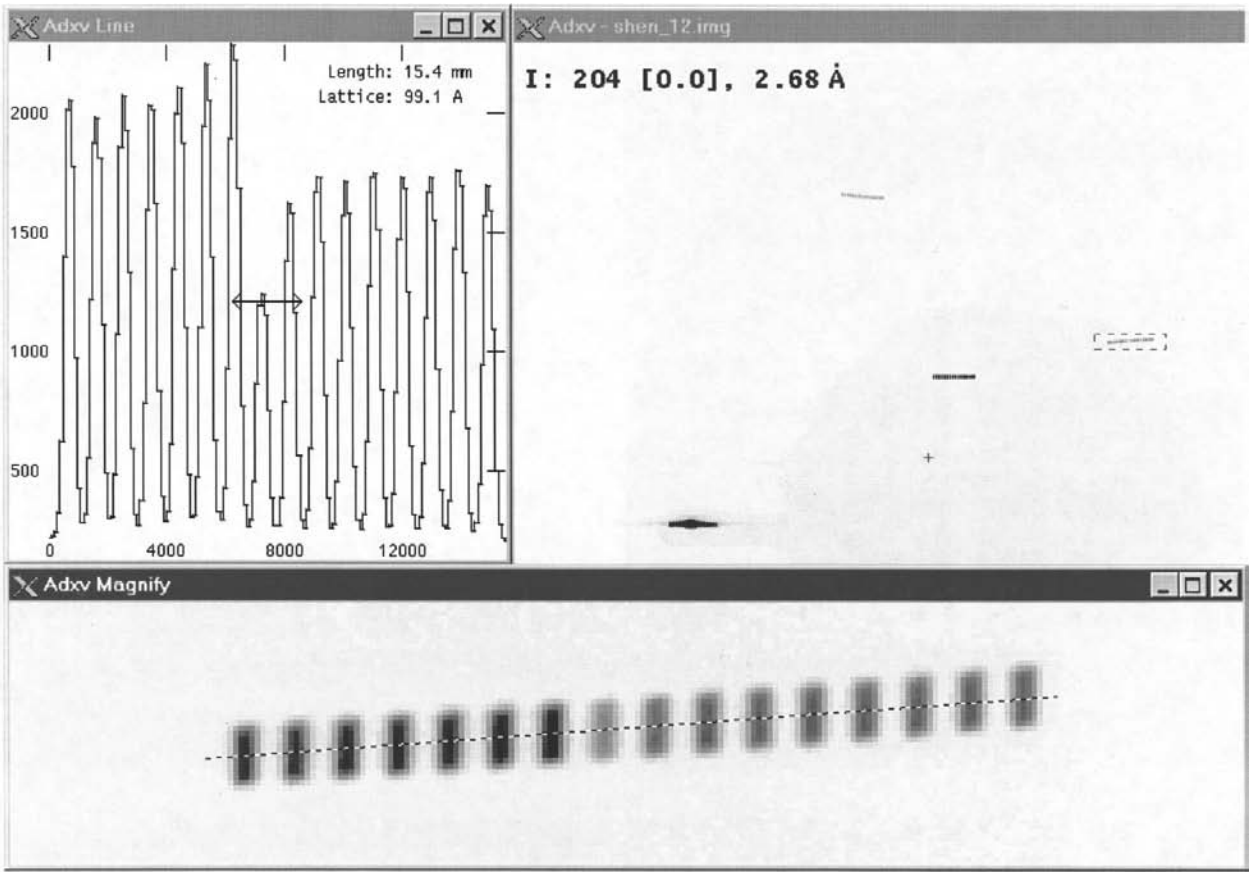

Figure 4
The first reference-beam diffraction oscillation image taken on a GaAs crystal using an image plate. The oscillation range was 20° and the exposure time was 40 s at each θ step. The interference profile along the 16 multiple exposures (with θ increasing from right to left) can be seen for all recorded reflections. Similar profiles have been observed by varying the incident X-ray energy (by 30 eV in 2 eV steps) instead of the rocking angle.

through a double-scattering process ($\mathbf{O}\rightarrow\mathbf{G}\rightarrow\mathbf{H}$) occurs only in *higher-order* triple-scattering processes ($\mathbf{O}\rightarrow\mathbf{H}\rightarrow\mathbf{G}\rightarrow\mathbf{H}$) in the case of reference-beam diffraction if an incident beam is purely $\boldsymbol{\sigma}$ polarized for the reference reflection **G**. This has been demonstrated through the second-order Born approximation (Shen, 1998). Since triple scattering is intrinsically weaker than double-scattering processes, a practical implication of lacking polarization mixing in double scattering in RBD is that it greatly reduces the effect of asymmetry reversal in the interference profiles that may exist in the conventional MBD measurements (Juretschke, 1984). This may therefore increase the reliability of the RBD phase measurements.

3. Experiments

We have demonstrated the RBD technique both on small-molecule crystals (Shen, 1998) and on real but good-quality biological crystals such as tetragonal lysozyme (Shen, 1999*a*). Typically, we use unfocused monochromatic 10–13 keV synchrotron X-rays as the incident beam, with an Si (111) double-crystal monochromator followed by a mirror for harmonic rejection. We use a standard four-circle diffractometer for specimen orientation, an oscillation camera set-up for exposure controls and an image plate or a CCD as the area detector for data collection.

3.1. Experiment on GaAs (004)

The first reference-beam diffraction image was obtained at the CHESS C1 station in June 1997 using a GaAs crystal with $\mathbf{G} = (004)$ as the reference reflection (Shen, 1998). The (004) reflection was aligned to be parallel to the oscillation axis by adjusting the two orthogonal cradles on a standard goniometer head. The RBD data were recorded on an image plate that was operated in 'streak-camera' mode in order to minimize the read-out errors for multiple exposures. The raw data image is shown in Fig. 4 through the ADXV software. The RBD interference profiles of all recorded Bragg reflections are clearly visible in the image, as shown by the intensity variations along the 16 multiple exposures taken as the rocking angle θ is stepped through the (004) rocking curve. The measured interference profiles agree very well with the theoretical calculations using either the *n*-beam dynamical theory (Colella, 1974) or the second-order Born approximation equation (3) (Shen, 1998).

3.2. Lysozyme experiments with image plates

The experiments on tetragonal lysozyme aimed both to test out the feasibility of the RBD method for small proteins and to develop a practical procedure for measurements and data analysis. Initial experiments on lysozyme were performed at CHESS C1 and F3 bent magnet stations, again using an image plate in streak-camera mode (Shen, 1999*a*). A typical diffraction image with $\mathbf{G} = (320)$, shown in Fig. 5, contains nine θ steps with a 10 s exposure per step for 1° oscillation range. It

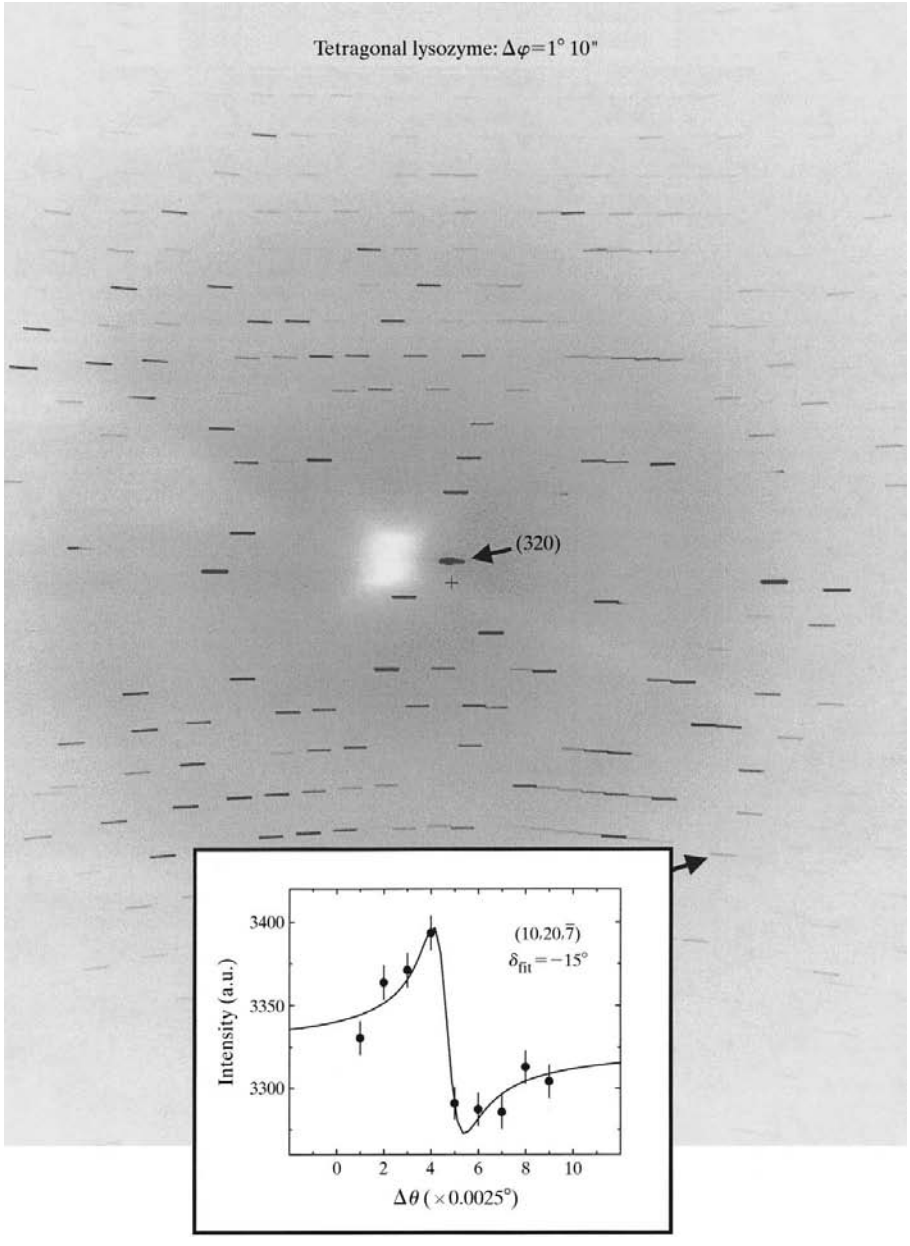

Figure 5
Reference-beam diffraction data on a tetragonal lysozyme with $\mathbf{G} = (320)$, using an image plate. The inset shows an example of the interference profile of one of the reflections as indicated by the arrow. The horizontal axis in the inset represents the sequence number of $\Delta\theta$ steps in 0.0025° increments.

was found that the RBD interference profiles, even though much weaker than small-molecule cases, were nevertheless detectable for as many as 20% of the diffraction spots. An example of such profiles is shown in the inset of Fig. 5. These profiles were then fit with an equation based on (3) and the triplet phases were obtained as the best fit values of δ.

3.3. Lysozyme experiments with CCD

One apparent drawback of using image plates in streak-camera mode is the artificially increased high background owing to the multiple exposures on the same plate during the RBD data collection. This would reduce the number of measurable weaker reflections at higher resolutions. The best way to solve this problem is to use a CCD detector (Fig. 6) that has a larger dynamic range (16 bit intensity scale on the ADSC Quantum-1 CCD *versus* 10 bit logarithmic scale on Fuji image plates) and can be used for multiple exposures controlled electronically. These experiments were performed at the A2 and C1 stations of CHESS and some examples of the results are shown in Fig. 7, which exhibit better quality RBD profiles owing to the increased number of θ steps and longer exposure times – 15 s per degree of oscillation at A2 wiggler station.

It is convenient and important in a RBD measurement to record the reference reflection intensity on the same θ image series so that a true rocking curve of the **G** reflection is measured simultaneously. This would indicate both the center $\theta_{\mathbf{G}}$ and the width Δ of the rocking curve that are needed for triplet-phase data analysis. Unfortunately, since **G** is a strong reflection and is aligned along the oscillation axis, its intensity usually oversaturates the pixels on the image plate or the CCD.

To overcome this problem, we have installed a small thin attenuator positioned around the **G** reflected beam next to the direct-beam stop in front of the area detector, as indicated by the shadows in the CCD images shown in Fig. 8. The thickness of the attenuator is adjusted at the peak of the **G** rocking curve to prevent intensity saturation. As illustrated in Fig. 7(*a*), this method has allowed us to faithfully record the reference-reflection intensities simultaneously with the RBD profiles, which is similar to the rocking-curve measurements in X-ray standing-wave experiments (Batterman, 1964; Bedzyk *et al.*, 1984).

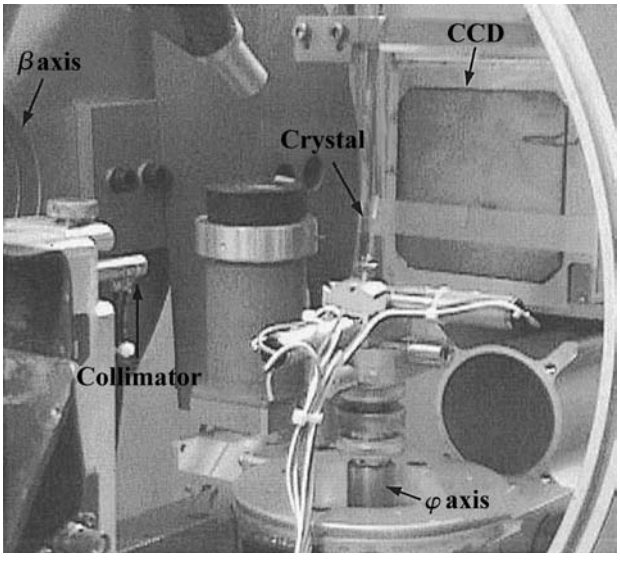

Figure 6
Reference-beam diffraction set-up using a CCD detector on a standard four-circle diffractometer. A DC-motor-controlled goniometer head is used to align a reference reflection onto the φ oscillation axis.

3.4. Inverse-beam measurements

In order to obtain enantiomorphic information for noncentrosymmetric crystals and to study the phase-insensitive *Umweganregung* and *Aufhellung* effects (Chang *et al.*, 1991, 1999; Weckert *et al.*, 1993; Weckert & Hümmer, 1997), we have performed inverse-beam RBD measurements of Friedel pairs, (**H**, **G**, **H**−**G**) and (−**H**, −**G**, **G**−**H**). On a

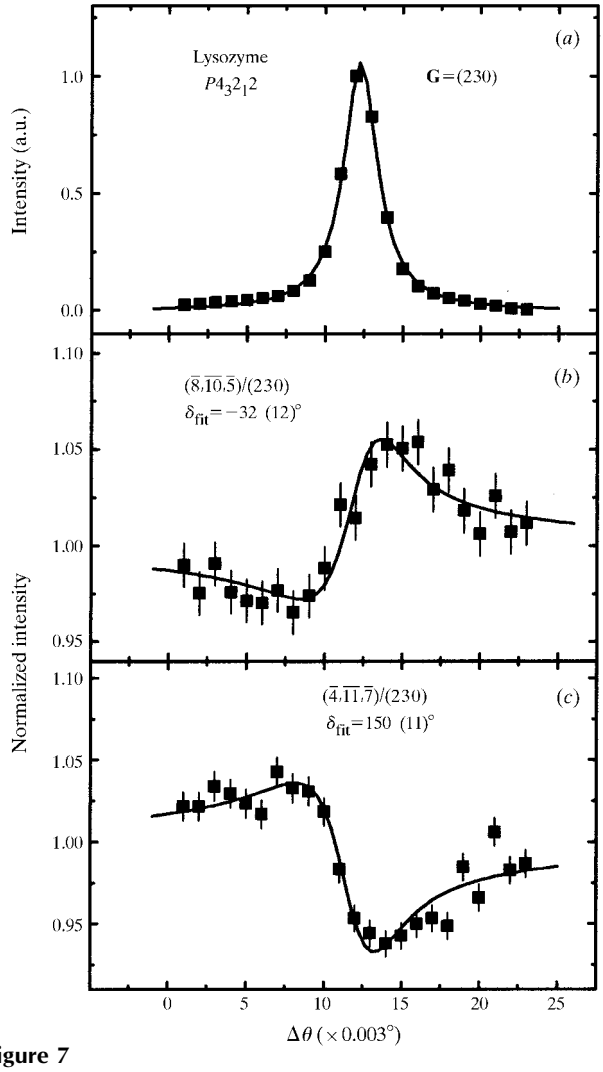

Figure 7
Two examples of the measured reference-beam diffraction profiles using a CCD detector, along with the rocking curve of the reference reflection **G** = (230) shown in (*a*). The solid curves in (*b*) and (*c*) are best fits to the data using equation (3) from which triplet phase values $\delta_{\rm fit}$ can be obtained. The rocking curve is fit with a Lorentzian.

standard four-circle diffractometer, the inverse RBD condition can be reached by rotating φ to $\varphi+180^\circ$ and χ to $\chi+180^\circ$ simultaneously (Shen *et al.*, 1999, 2000). This operation is equivalent to a single rotation of θ to $\theta+180^\circ$ as normally performed in multiple-wavelength anomalous diffraction (MAD) experiments. The 180° θ rotation was not possible in the RBD geometry owing to the various spatial constraints on the existing four-circle diffractometer.

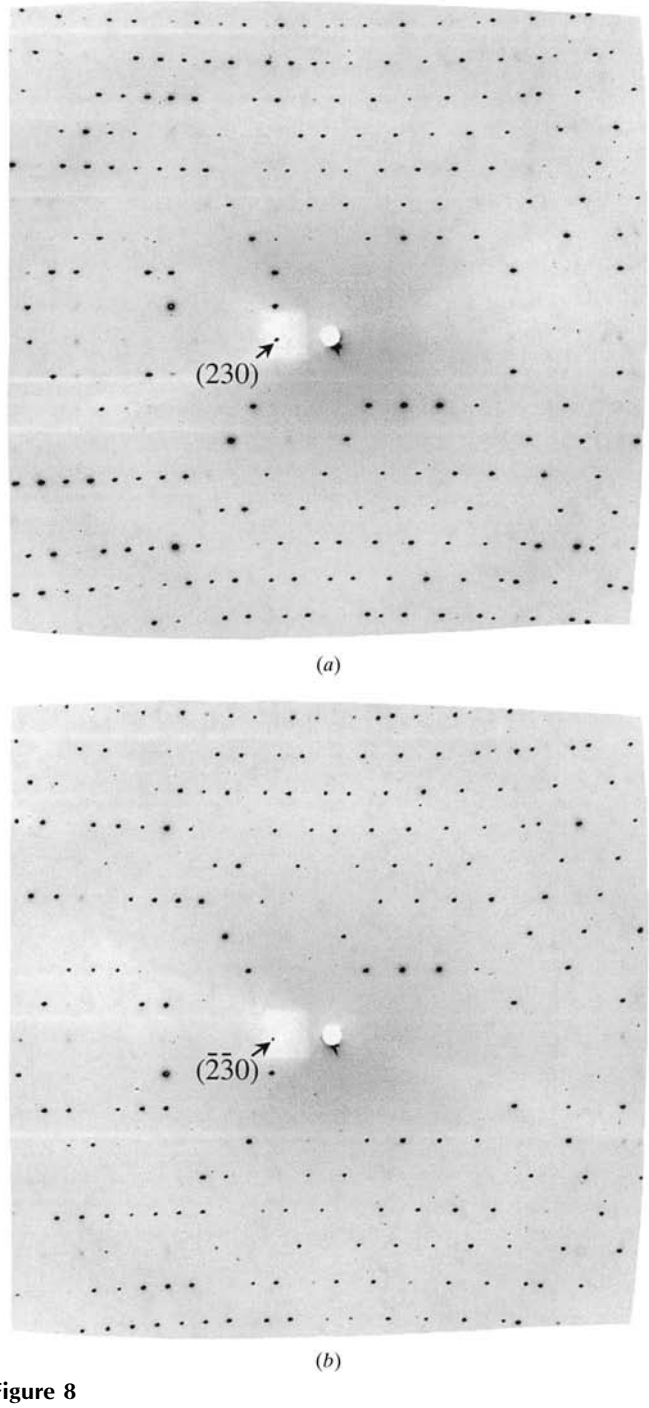

Figure 8
Inverse-beam related reference-beam diffraction patterns on tetragonal lysozyme using a CCD detector, (*a*) **G** = (230) and (*b*) **G** = ($\bar{2}\bar{3}0$), which are mirror images of each other.

As shown in Fig. 8, the two inverse-beam diffraction images for the same oscillation range $\Delta\varphi$ are related by a mirror reflection. Automatic indexing with standard crystallographic programs such as *DENZO* (Otwinowski & Minor, 1997) confirms that all reflections recorded in the two frames are related by Friedel pairs. An example of the RBD profiles of a Friedel pair, ($3\bar{2}4$)/(230) and ($\bar{3}2\bar{4}$)/($\bar{2}\bar{3}0$), is shown in Fig. 9. Measurements such as this allow an unambiguous distinction of the enantiomorphic space groups, $P4_32_12$ or $P4_12_12$ in the case of lysozyme (Shen *et al.*, 1999, 2000), and thus absolute structures can be determined in the absence of anomalous signals as already demonstrated with the conventional multiple-beam diffraction technique (Shen & Finkelstein, 1990; Weckert *et al.*, 1993; Colella, 1995*b*).

3.5. Results on a quasicrystal

In addition to macromolecular crystals, the RBD technique can be useful for other material systems in which the diffraction phase problem exists. An example is an intermetallic quasicrystal, which is a unique class of materials with no periodic unit cell yet can produce sharp diffraction peaks in an

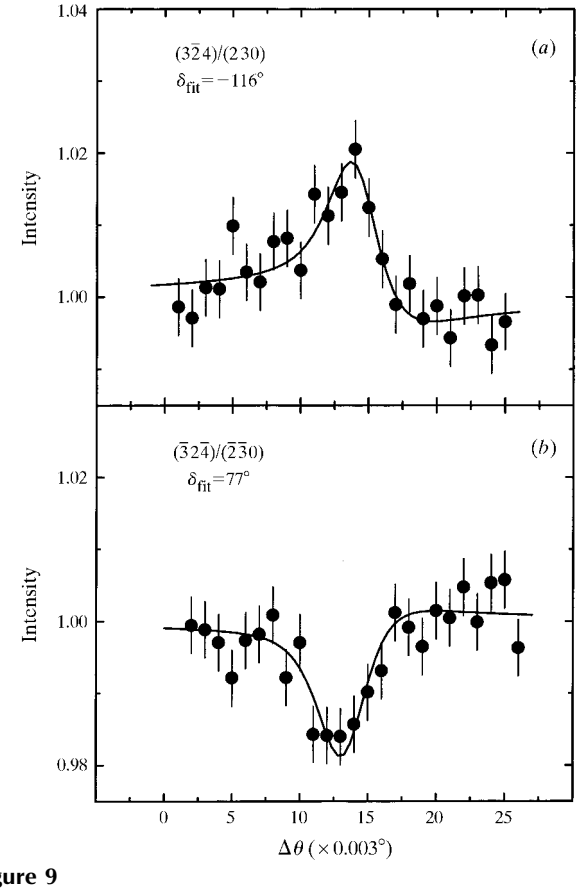

Figure 9
Reference-beam diffraction profiles of a Friedel pair on lysozyme, (*a*) **H** = ($3\bar{2}4$), **G** = (230), and (*b*) **H** = ($\bar{3}2\bar{4}$), **G** = ($\bar{2}\bar{3}0$), recorded in inverse-beam reference-beam measurements. The curves are the best fits to the data using equation (3) from which triplet-phase values of $\delta_{\rm fit} = -116\ (8)^\circ$ for the ($3\bar{2}4$) and $\delta_{\rm fit} = 77\ (8)^\circ$ for the ($\bar{3}2\bar{4}$) are obtained.

X-ray diffraction experiment. These peaks are generally indexed by six integers representing a six-dimensional reciprocal space. To date, only a few attempts have been made towards finding a solution to the phase problem for quasicrystal structures (Lee *et al.*, 1996; Zhang *et al.*, 1998; for a recent review, see Elser, 1999).

To help solve this problem, we have performed a reference-beam diffraction experiment on an AlPdMn quasicrystal. The reference reflection used in our experiment was a $\mathbf{G} = (0120\bar{1}2)$ twofold reflection (20/32 reflection). The RBD data are recorded with a CCD detector. In Fig. 10, we show a typical diffraction image with an oscillation range of $\Delta\varphi = 16^\circ$ and an exposure time of 40 s at each θ step. The inset shows the RBD profile of one of the reflections, $\mathbf{H} = (\bar{1}12\bar{1}\bar{1}2)$, where the interference effect can be clearly seen. In addition to the Bragg peaks, significant diffuse scattering signals are also recorded on the same image, which exhibit in some cases a pentagon-shaped contour. A more complete data analysis is in progress and the results will be reported in a future article.

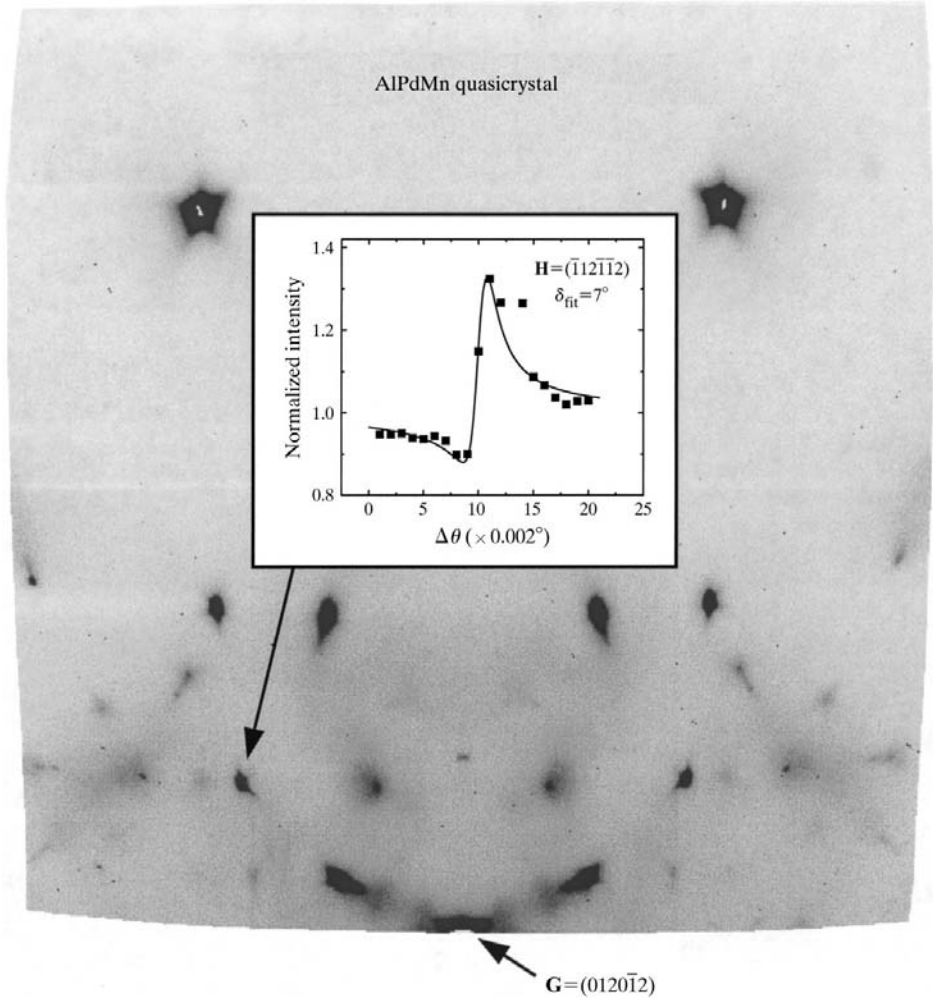

Figure 10
An example of the reference-beam diffraction pattern from an AlPdMn quasicrystal recorded on a CCD, with intensities in gray linear scale. The interference profile of one of the reflections is shown in the inset.

4. Data processing

With the aim to make RBD a real practical technique that can be used not only by X-ray specialists but also by crystallographers with a broad range of backgrounds, we have devoted considerable efforts to RBD data processing and analyses and have developed a procedure that would automatically extract the triplet-phase values for a large number of Bragg reflections collected in a RBD experiment. This procedure consists of the following principal steps.

4.1. Indexing, integration and scaling

The first step in analyzing a series of RBD images is to index the oscillation pattern. Even though each image is obtained by rotating the crystal around an axis that is not perpendicular to the incident beam, we have found that the existing crystallographic software packages such as *DENZO* (Otwinowski & Minor, 1997) and *DPS* (Steller *et al.*, 1997) can be reliably used for automatically indexing a RBD pattern. This procedure can also be used to obtain an initial orientation matrix for alignment of the reference reflection.

With a diffraction pattern indexed, integrated intensities of each Bragg reflection are evaluated, for each θ step, using the same software package, to provide a series of integrated intensities $I_{\mathbf{H}}(\theta)$. These intensities are then scaled using *ScalePack* in the CCP4 package (Collaborative Computational Project, Number 4, 1994) to take into account the incident-beam variations among other experimental factors. We have found that the automatic scaling function in the package provides results that agree very well with the experimentally measured incident-beam monitor counts, although the latter have been used in almost all cases in our analyses. The end result of this step is a series of properly scaled integrated intensities $I_{\mathbf{H}}(\theta)$, not merged among the symmetry-related peaks, of all recorded Bragg reflections in the experiment.

4.2. Curve fitting for triplet phases

The second step in the RBD data analysis is to extract the triplet-phase values δ from the $I_{\mathbf{H}}(\theta)$ data profiles. To do this automatically with minimal operator intervention, we have developed a curve-fitting program to fit the $I_{\mathbf{H}}(\theta)$ data series to a RBD interference function, equation (3) or

(5), which can directly yield the best-fit values of δ for all recorded reflections, as already illustrated in Figs. 7, 9 and 10.

The fitting function we have used so far has been entirely based on the result from the second-order Born approximation, equation (3). With $R_{\mathbf{G}}(\theta)$ substituted by a Lorentzian and $\nu_{\mathbf{G}}(\theta)$ by equation (4), the fitting function is defined as the following:

$$I_{\mathbf{H}}(\theta) = C + \left(p/\{1 + [(\theta - \theta_{\mathbf{G}})/\Delta]^2\}^{1/2}\right) \cos[\delta + \nu_{\mathbf{G}}(\theta)], \quad (9)$$

which involves only four fitting parameters: base intensity C, peak of the interference term p, center of the rocking curve $\theta_{\mathbf{G}}$ and, finally, triplet phase δ. The half width Δ of the rocking curve is usually taken from the experimental measurements. Even though its center $\theta_{\mathbf{G}}$ is also known from a simultaneously measured rocking curve, we allow $\theta_{\mathbf{G}}$ to vary within a narrow region of $\pm\Delta$ to account for theoretical approximations involved in arriving at equation (9), as well as possible experimental errors. In some cases, a fifth parameter is used to take into account a sloped baseline intensity, which may exist when the peak is a partial reflection.

4.3. Rejection of unreliable phases

Finally, it should be pointed out that fitting all recorded RBD intensity series automatically does not mean that every reflection exhibits the true reference-beam interference pattern. The second step outlined above is merely part of an automated procedure and the next step is to develop a goodness-of-fit criterion that would allow us to reject the bad intensity profiles that for various reasons do not actually contain the true interference information.

Contrary to some of the existing criteria on observable multiple-beam interference effects based on magnitude ratios of the involved structure factors (Weckert & Hümmer, 1997), the rejection criteria that have been developed for the RBD analysis rely mostly on the error assessments of the experimental measurements through curve fitting to equation (9). The criteria established this way depend on, *e.g.*, the χ^2 value of the best fit, the error bar of fitting parameter δ, the magnitude of p and whether $\theta_{\mathbf{G}}$ is at its boundary.

To illustrate this procedure, we show in Fig. 11 a comparison of measured triplet phases of tetragonal lysozyme with the calculated phases based on a data entry in the Protein Data Bank (Vaney *et al.*, 1995). The histogram or occurrence distribution as a function of phase error, defined as the difference between the measured and the calculated phases, of all 1317 measured triplet phases with $\chi^2 > 0$ resulted from the curve-fitting step is shown as squares, with the solid curve as a guide to the eye. The distribution can be viewed as a Gaussian peak centered at zero, which contains the true phase information, on a randomly distributed background. We then apply a rejection criterion that eliminates all measured phases with the error bars on δ greater than 45° *and* with the center $\theta_{\mathbf{G}}$ at its boundaries of the allowed range. As a result, this procedure drastically reduces the random background in the distribution while it retains the Gaussian peak to a large degree, as shown by the circles in Fig. 11. The final 513 triplet phases obtained in this way have a median phase error of 54° and are much more reliable than the whole data set. It is expected that the reliability of the measured triplet phases can be increased further once the inverse-beam measurements of Friedel pairs (Shen *et al.*, 1999, 2000) are fully integrated into the data analysis. Further constraints on symmetry-related and/or redundant reflections may also be incorporated, which may lead to additional rejection criteria or to more accurate phase values.

With the automated data-processing steps outlined above, a large number of experimentally measured triplet phases are deduced along with their weighting factors that indicate the reliability of the phases. These phases obtained in RBD experiments can then be used in existing phasing programs such as those based on direct methods (Weeks *et al.*, 1999, 2000), or in other possible algorithms proposed with conventional MBD data (Mo *et al.*, 1996; Weckert & Hümmer, 1997; Mathiesen & Mo, 1998), to solve the crystal structure of the specimen.

5. Discussion and conclusions

There are several significant practical advantages of the RBD technique over the traditional ψ-scan method for multiple-beam diffraction. First, of course, the parallel data-collection method of RBD allows the measurements of many three-

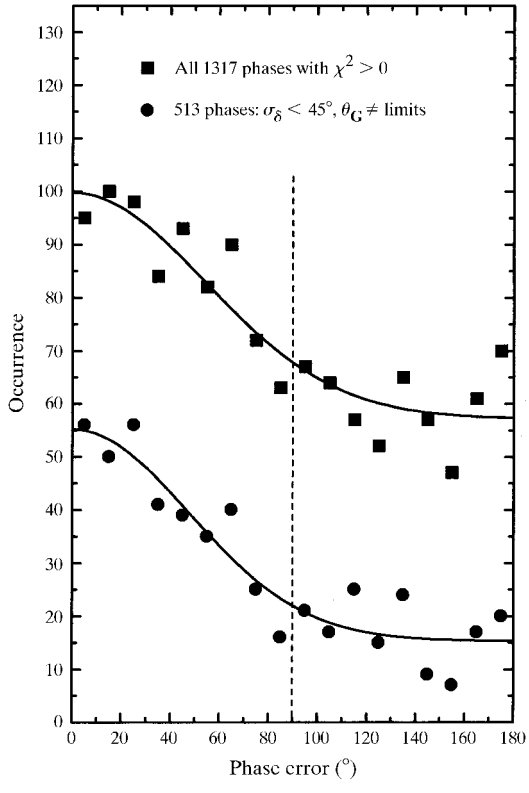

Figure 11
Histogram distribution of measured triplet phases *versus* the phase error, defined as the difference between the measured and the calculated triplet phases. The squares represent all phases resulting from the automatic curve fitting and the circles represent a final set of phases after the rejection criterion is applied as indicated. The solid curves are fits to a Gaussian plus a random background.

beam profiles to be performed in a much shorter time than the traditional method, which can therefore minimize the effect of crystal radiation damage at a synchrotron source. Second, since the reference **G** serves as the common detour reflection, the dynamical phase shift $\nu_{\mathbf{G}}$ is well defined for a given rocking-angle direction and no ambiguities exist as in the case of the ψ-scan technique where two situations, 'in' or 'out' (Chang, 1982, 1998), need to be distinguished. Third, as already mentioned in §2, there are no polarization switching factors in reference-beam geometry if the incident beam is purely or mostly $\boldsymbol{\sigma}$ polarized for the **G** reflection, which is most likely the case at a synchrotron source. Finally, it is possible that a larger out-of-plane horizontal divergence in the incident beam can be tolerated in a RBD experiment compared to the ψ-scan method. This fits the natural beam divergence of a synchrotron beam very well.

In terms of data-collection procedures, the RBD method presented here is very similar to multiple-wavelength anomalous diffraction (MAD) experiments. Here the angular setting of the reference reflection **G** serves the same role as the atomic absorption-edge energy of a heavy atom. Multiple oscillation data sets are collected around the Bragg angle $\theta_{\mathbf{G}}$, much like those around the absorption edge, with similar useful signal levels of a few percent for proteins. In fact, instead of changing the rocking angle θ, one can change the incident energy to pass through the reference-reflection rocking curve and take multiple data sets at several energies, as mentioned in Fig. 4. An additional advantage is that no global scaling is necessary in RBD measurements so that incomplete data sets from different crystals can easily be combined. This advantage may be significant since radiation damage of biological samples is of serious concern in many crystallography experiments.

As for how the measured phase information is used to help to solve a crystal structure, the algorithms for the RBD data sets are probably different from the MAD technique. So far, the most promising route to utilize the RBD measured phases is to incorporate the phase information into the traditional or dual-space direct-methods algorithms (Weeks *et al.*, 1998; Hauptman *et al.*, 1999). One interesting question that needs to be addressed is the following. Given the way a RBD experiment is performed, there is very little overlap among the individual structure-factor phases in a given data set involving a single reference reflection **G**. Therefore, how many such data sets with different **G**'s, either complete or partial, does one need to solve a realistic structure? Preliminary simulations by Weeks *et al.* (1999, 2000) using a unified *Shake-and-Bake* program (Miller *et al.*, 1993) suggest that a structural solution is possible for a small protein (crambin) with even a single measured phase data set (single **G**) if the data set is rather complete (though less than atomic resolution) and accurate with a measurement error of less than 20° or so in the measured triplet phases. The tolerance on the phase errors can be as high as 50° if three or more RBD data sets are measured. These preliminary results are encouraging but further studies are needed to reach a general conclusion.

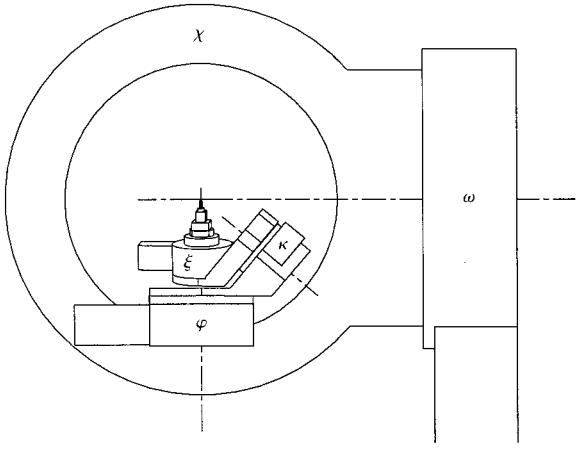

Figure 12
Schematic drawing of a new five-circle diffractometer design for reference-beam diffraction experiment, where an additional κ-goniometer (κ, ξ) mounted on the oscillation φ axis allows an easy alignment of any Bragg peak used as the reference reflection. An incident beam would be along the direction out of the page in this drawing.

In addition to theoretical strategies, several challenging issues need to be resolved in experiments before the RBD technique can be widely adopted in everyday crystallography. In order to speed up the initial alignment of a reference reflection for an arbitrary crystal system, we have designed and constructed a special computer-controlled κ goniometer that can be mounted on the φ stage of a standard four-circle diffractometer (Fig. 12). With this five-circle κ set-up, one can automatically orient any Bragg reflection along φ, which serves as the crystal oscillation axis. This eliminates one of the time-consuming steps in a RBD experiment. Other experimental problems include how to handle increased crystal mosaicity on freezing specimens, how to minimize the effects of overlapping multiple reflections for larger structures, and how to improve the intensity integration statistics on area detectors for better data accuracy. Even though the accuracy of the RBD-measured triplet phases may never be able to approach that of using the traditional ψ-scanning method and a point detector (Weckert & Hümmer, 1997), it is entirely possible that its measurement errors would be somewhat compensated by the large number of measured phases that can be used in structural determination routines.

In summary, we have demonstrated that the reference-beam diffraction technique is a promising and practical approach of solving the phase problem in X-ray crystallography, without the need for heavy-atom derivatives. By incorporating the principle of three-beam diffraction into the standard oscillating-crystal data-collection technique and by a recently developed automated data-reduction procedure, a large number of Bragg-reflection triplet phases can be measured in a RBD experiment using an area detector within a relatively short time period. With further research and development, we believe that the new method will have a significant impact on crystallography data collection and structural determinations.

The authors would like to acknowledge J. LaIuppa, P. Doing, M. Szebenyi, C. Heaton, W. Miller and K. Finkelstein for

participating and helping in the experiments. Thanks are due to B. Batterman, E. Fontes, S. Ealick, D. Thiel, R. Thorne and S. Gruner at Cornell, as well as R. Colella and M. Rossmann at Purdue for useful discussions. Collaborations with H. Hauptman, C. Weeks, H. Xu and others at the Hauptman–Woodward Institute are also greatly appreciated. This work is supported by NSF through CHESS under Grant DMR 97-13424.

References

Authier, A. (1986). *Acta Cryst.* A**42**, 414–426.
Batterman, B. W. (1964). *Phys. Rev.* **133**, A759–A764.
Batterman, B. W. & Cole, H. (1964). *Rev. Mod. Phys.* **36**, 681–717.
Bedzyk, M. J., Materlik, G. & Kovalchuk, M. V. (1984). *Phys. Rev. B*, **30**, 2453–2461.
Caticha-Ellis, S. (1975). *Jpn. J. Appl. Phys.* **14**, 603–611.
Chang, S. L. (1982). *Phys. Rev. Lett.* **48**, 163.
Chang, S. L. (1984). *Multiple Diffraction of X-rays in Crystals.* New York: Springer Verlag.
Chang, S. L. (1998). *Acta Cryst.* A**54**, 886–894.
Chang, S. L., Chao, C. H., Huang, Y. S., Jean, Y. C., Sheu, H. S., Liang, F. J., Chien, H. C., Chen, C. K. & Yuan, H. S. (1999). *Acta Cryst.* A**55**, 933–938.
Chang, S. L., King, H. E. Jr, Huang, M-T. & Gao, Y. (1991). *Phys. Rev. Lett.* **67**, 3113.
Chapman, L. D., Yoder, D. R. & Colella, R. (1981). *Phys. Rev. Lett.* **46**, 1578–1581.
Cole, H., Chambers, F. W. & Dunn, H. M. (1962). *Acta Cryst.* **15**, 138–144.
Colella, R. (1974). *Acta Cryst.* A**30**, 413–423.
Colella, R. (1995*a*). *Comments Condens. Mater. Phys.* **17**, 175–215.
Colella, R. (1995*b*). *Acta Cryst.* A**51**, 438–440.
Collaborative Computational Project, Number 4 (1994). *Acta Cryst.* D**50**, 760–763.
Dietrich, S. & Wagner, H. (1984). *Z. Phys. B*, **56**, 207.
Elser, V. (1999). *Acta Cryst.* A**55**, 489–499.
Giacovazzo, C., Siliqi, D. & Ralph, A. (1994). *Acta Cryst.* A**50**, 503–510.
Hart, M. & Lang, A. R. (1961). *Phys. Rev. Lett.* **7**, 120–121.
Hauptman, H. A., Weeks, C. M., Xu, H. & Shen, Q. (1999). XVIIIth IUCr Congress, Glasgow, Scotland, Abstract P12.02.012
Hendrickson, W. (1991). *Science*, **254**, 51.
Juretschke, H. J. (1982). *Phys. Rev. Lett.* **48**, 1487–1489.
Juretschke, H. J. (1984). *Acta Cryst.* A**40**, 379–389.
Lee, H., Colella, R. & Shen, Q. (1996). *Phys. Rev. B*, **54**, 214–221.
Mathiesen, R. H. & Mo, F. (1998). *Acta Cryst.* D**54**, 237–242.
Mathiesen, R. H., Mo, F., Eikenes, A., Nyborg, T. & Larsen, H. B. (1998). *Acta Cryst.* A**54**, 338–347.
Miller, R., DeTitta, G. T., Jones, R., Langs, D. A., Weeks, C. M. & Hauptman, H. A. (1993). *Science*, **259**, 1430.
Mo, F., Mathiesen, R. H., Hauback, B. C. & Adman, E. T. (1996). *Acta Cryst.* D**52**, 893–900.
Otwinowski, Z. & Minor, W. (1997). *Methods Enzymol.* **276**, 307–326.
Post, B. (1977). *Phys. Rev. Lett.* **39**, 760–763.
Schmidt, M. C. & Colella, R. (1985). *Phys. Rev. Lett.* **55**, 715–718.
Shen, Q. (1986). *Acta Cryst.* A**42**, 525–533.
Shen, Q. (1993). *Acta Cryst.* A**49**, 605–613.
Shen, Q. (1998). *Phys. Rev. Lett.* **80**, 3268–3271.
Shen, Q. (1999*a*). *Phys. Rev. B*, **59**, 11109–11112.
Shen, Q. (1999*b*). *Phys. Rev. Lett.* **83**, 4784–4787.
Shen, Q. (1999*c*). In *Methods in Materials Research*, edited by E. N. Kaufmann. New York: Wiley. In the press.
Shen, Q. & Colella, R. (1987). *Nature (London)*, **329**, 232–233.
Shen, Q. & Finkelstein, K. D. (1990). *Phys. Rev. Lett.* **65**, 3337–3340.
Shen, Q. & Finkelstein, K. D. (1992). *Phys. Rev. B*, **45**, 5075–5078.
Shen, Q., Kycia, S. & Dobrianov, I. (1999). XVIIIth IUCr Congress, Glasgow, Scotland, Abstract 07.OA.005.
Shen, Q., Kycia, S. & Dobrianov, I. (2000). *Acta Cryst.* A**56**, 264–267.
Sinha, S. K., Sirota, E. B., Garoff, S. & Stanley, H. B. (1988). *Phys. Rev. B*, **38**, 2297.
Steller, I., Bolotovsky, R. & Rossmann, M. G. (1997). *J. Appl. Cryst.* **30**, 1036–1040.
Tegze, M. & Faigel, G. (1996). *Nature (London)*, **380**, 49.
Thorkildsen, G. (1987). *Acta Cryst.* A**43**, 361–369.
Thorkildsen, G. & Larsen, H. B. (1998). *Acta Cryst.* A**54**, 120–128.
Tischler, J. Z. & Batterman, B. W. (1986). *Acta Cryst.* A**42**, 510–514.
Vaney, M. C., Maignan, S., Ries-Kautt, M. & Ducruix, A. (1995). Protein Data Bank, PDB ID = 193L.
Vineyard, G. H. (1982). *Phys. Rev. B*, **26**, 4146.
Weckert, E. & Hümmer, K. (1997). *Acta Cryst.* A**53**, 108–143.
Weckert, E., Schwegle, W. & Hümmer, K. (1993). *Proc. R. Soc. London Ser. A*, **442**, 33–46.
Weeks, C. M., Miller, R. & Hauptman, H. A. (1998). *Direct Methods for Solving Macromolecular Structures*, edited by S. Fortier, pp. 463–468. Dordrecht: Kluwer Academic Publishers.
Weeks, C. M., Xu, H., Hauptman, H. A. & Shen, Q. (1999). Am. Crystallogr. Assoc. Annual Meeting, Buffalo, NY, USA, Abstract PT10.
Weeks, C. M., Xu, H., Hauptman, H. A. & Shen, Q. (2000). *Acta Cryst.* A**56**, 280–283.
Zachariasen, W. H. (1945). *Theory of X-ray Diffraction in Crystals.* New York: Dover.
Zhang, Y., Colella, R., Shen, Q. & Kycia, S. W. (1998). *Acta Cryst.* A**54**, 411–415.